

# Towards Lasing Without Inversion in Neutral Mercury

**Benjamin Rein, Martin R. Sturm, Reinhold Walser and Thomas Walther**

Institute for Applied Physics, TU Darmstadt, Schlossgartenstr. 7, D-64289 Darmstadt

E-mail: [thomas.walther@physik.tu-darmstadt.de](mailto:thomas.walther@physik.tu-darmstadt.de)

**Abstract.** Currently, we are implementing a lasing without inversion (LWI) scheme in mercury based on calculations by Fry *et al.* [1]. A recent detailed analysis predicting exact experimental parameters shows the feasibility of our LWI scheme [2]. In this paper we report on the progress of our experiment and compare its parameters with the prior analysis.

## 1. Introduction

The development of cw lasers in the UV and VUV wavelength regions is a very active field of research as there are many applications, e.g. in quantum information processing, biomedicine and laser lithography [3, 4]. However, this development remains a challenging task, particularly since the pump power required for a population inversion at the laser transition scales at least with the laser frequency  $\omega^4$  and therefore makes it hard to build conventional lasers in this regime [5]. Common methods to generate continuous-wave laser radiation in the UV are second and fourth harmonic generation [6]. However, second and fourth harmonic generation are limited by the availability of materials transparent in the VUV. An alternative is four-wave mixing which even makes it possible to generate light in the VUV region [7]. All of these techniques exploit nonlinear effects.

A different approach is lasing without inversion (LWI) based on the coherent excitation of atomic transitions. It was first proposed in [8, 9, 10]. The main idea is to cancel the absorption of radiation on the lasing transition such that a few incoherently excited atoms are sufficient to achieve gain by stimulated emission of radiation. Successful demonstrations of continuous-wave LWI were shown in rubidium [11] and sodium [12, 13], but until now there is no LWI scheme where the lasing transition has a significantly shorter wavelength than the lasers used to generate the coherent excitation. The overall objective of our project is to generate a UV source based on LWI in neutral mercury. In this contribution we report on the experimental progress towards this goal.

In our experimental implementation, we employ an LWI scheme in mercury which was first proposed by Fry *et al.* [1]. In this scheme, the laser transition is at 253.7 nm and the shortest wavelength to build up the coherence is at 435.8 nm. Because of the 4-level structure and its favorable energy structure, it is even possible to cancel the Doppler effect, preventing the gain spike from being washed out.

In this paper, we present a short summary of new detailed calculations of LWI in mercury



which were carried out by Martin Sturm *et al.* [2] and give a status update of the experimental realization.

## 2. Theoretical model of LWI in mercury

The four-level scheme used for LWI in mercury is depicted in Fig. 1(a) and involves the  $6^1S_0$  ground state as well as the  $6^3P_1$  state and the metastable  $6^3P_2$  state which are connected through the  $7^3S_1$  state employing the strong driving laser at 435.8 nm as well as the weak coupling laser at 546.1 nm with the Rabi frequencies  $\Omega_s$  and  $\Omega_w$ , respectively. The laser transition at 253.7 nm is between the ground state  $6^1S_0$  and the excited state  $6^3P_1$  with  $\Omega_p$ . Because there could be population trapping into the metastable state  $6^3P_0$  an incoherent repumping laser at 404.7 nm is added, connecting the  $6^3P_0$  state to the  $7^3S_1$  state.

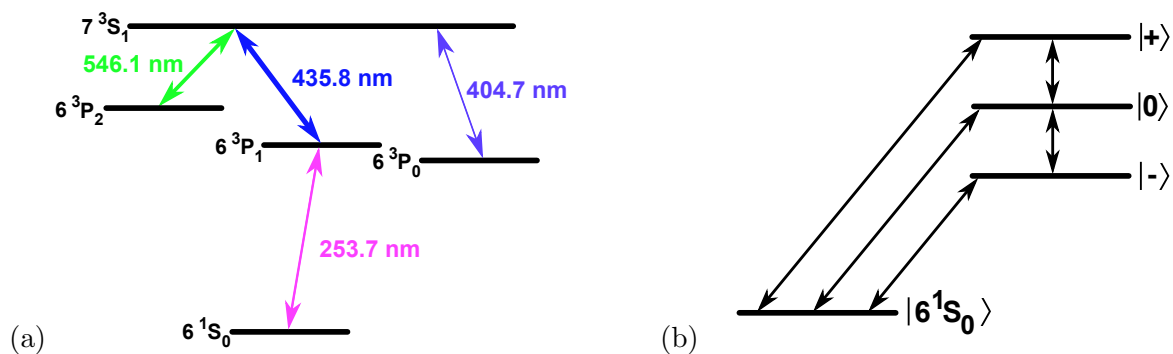


**Figure 1.** (a) Mercury level scheme used for LWI at 253.7 nm. See text for details. (b) Dressed-state picture of the four-level scheme in mercury with the Rabi frequencies of the coupling lasers  $\Omega_s$ ,  $\Omega_w$ . All detunings are assumed to be zero, i.e.  $\Delta_{s,w} = 0$ .

The Hamiltonian of this system in the dipole and rotating wave approximation is given by [2]

$$H = \begin{pmatrix} 0 & \Omega_p^* & \Omega_s & 0 \\ \Omega_p & -\Delta_p & 0 & 0 \\ \Omega_p^* & 0 & \Delta_s & \Omega_w^* \\ 0 & 0 & \Omega_w & \Delta_s - \Delta_w \end{pmatrix}, \quad (1)$$

in the basis of the atomic levels  $\{|6^3P_1\rangle, |6^1S_0\rangle, |7^3S_1\rangle, |6^3P_2\rangle\}$  and  $\Delta_{w,s,p}$  are the detunings of the lasers with respect to the corresponding atomic transitions. The origin of the LWI mechanism is easier to understand in the dressed-state picture. Therefore, we diagonalize the matrix and solve for the eigenvalues of the Hamiltonian:

$$|0\rangle = |6^3P_2\rangle - \frac{\Omega_w^*}{\Omega_s^*} |6^1S_0\rangle \quad (2)$$

$$|\pm\rangle = \frac{1}{\sqrt{2}} \left( |6^1S_0\rangle \mp \frac{|\Omega_s|}{\Omega_s} |7^3S_1\rangle + \frac{\Omega_w}{\Omega_s} |6^3P_2\rangle \right), \quad (3)$$

with all detunings  $\Delta_{w,s,p} = 0$  and  $\Omega_p = 0$ . The corresponding dressed-state picture is shown in Fig. 1(b). For a vanishing coupling laser,  $\Omega_w = 0$ , the  $|\pm\rangle$  states correspond to the usual Autler-Townes splitting in a three-state ladder system. With the coupling laser switched on, the dressed state  $|0\rangle$  consists of a mixture of the bare states  $|6^3P_2\rangle$  and  $|6^3P_1\rangle$  and couples to the ground state  $|6^1S_0\rangle$ . In the bare-state picture this corresponds to a three-photon transition

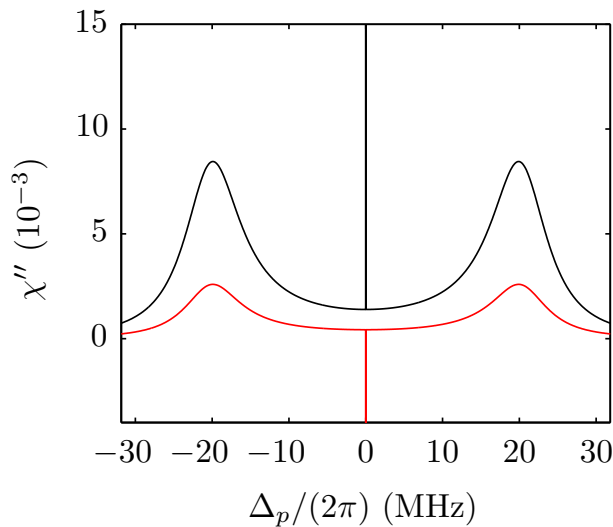


**Figure 2.** The imaginary part of the susceptibility  $\chi$ , which corresponds to the absorption on the laser transition, versus the detuning  $\Delta_p$  with enabled coupling lasers  $\Omega_s$  and  $\Omega_w$ . The black curve shows the absorption without an incoherent pump on the 253.7 nm transition. With the incoherent pump switched on (red curve), the sharp absorption spike at  $\Delta_p = 0$  turns into a gain spike [2].

between the ground state  $|6^1S_0\rangle$  and the upper state  $|6^3P_2\rangle$  and leads to a sharp absorption feature (cf. Fig. 2).

Fig. 2 shows a simulation of the imaginary part of the susceptibility of the laser transition at 253.7 nm, solving the Bloch equations and employing the natural line widths of the corresponding transitions of mercury. By irradiating an incoherent pump on the lasing transition, the sharp absorption feature becomes a gain spike which could lead to LWI (c.f. red curve in Fig. 2).

The particular advantage of the 4-level scheme for LWI becomes evident when Doppler broadening is taken into account [1]. The photon momenta corresponding to the drive, coupling lasers and laser transition fulfill the triangle equation, i.e. one can find a geometrical orientation of the laser beams such that the momenta fulfill the equation  $\vec{k}_p + \vec{k}_s - \vec{k}_w = 0$ . Thus, for this alignment the Doppler effect is canceled in one direction for the laser field at 253.7 nm (cf. Fig. 3). This allows a much simpler experimental setup as it becomes feasible to use gas cells rather than much more complicated atomic beam setups.

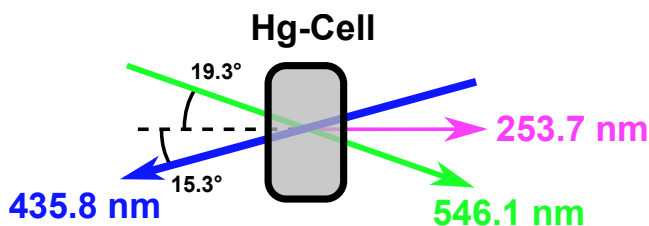


**Figure 3.** Geometrical orientation of the coupling lasers  $\Omega_s$  and  $\Omega_w$  such that the Doppler effect is canceled in one direction for the 253.7 nm laser field.

In order to arrive at a more realistic picture of the necessary experimental parameters, in the next step of the simulation we took into account the Doppler effect with respect to our particular alignment of the laser beams, the finite linewidths of the driving lasers and used the coupling scheme including all Zeeman sublevels and chose the polarization of the laser fields as proposed in [1]. The central part around the gain spike of the imaginary part of the susceptibility under these conditions is shown in Fig. 4. Clearly, the gain spike is dependent on atomic density, pump rate, the Rabi frequencies of the drive and coupling lasers as well as the linewidths of these two lasers. The latter is particularly striking as the dependence is very strong and for large linewidth the gain spike can even vanish. Thus, in an experimental implementation special attention must be paid to achieve the smallest possible linewidths for the corresponding laser radiation.

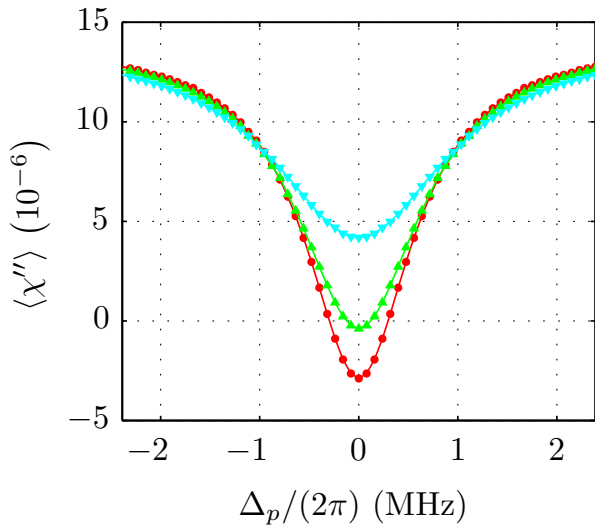


**Figure 4.** The imaginary part of the susceptibility  $\chi$  of the laser transition versus the detuning  $\Delta_p$  for different linewidths of the coupling lasers  $\Omega_s$  and  $\Omega_w$ . Red dots correspond to a linewidth of 0 kHz, green triangles to 8 kHz and cyan triangles to 32 kHz for both coupling lasers [2].

The simulations were extended to include the spatial dependence of the gain distribution for actual Gaussian beams (cf. Fig. 5). Based on these calculations with realistic laser parameters, it is possible to choose the optimal length of the mercury vapor cell in which the lasers are overlapped and form the LWI zone.

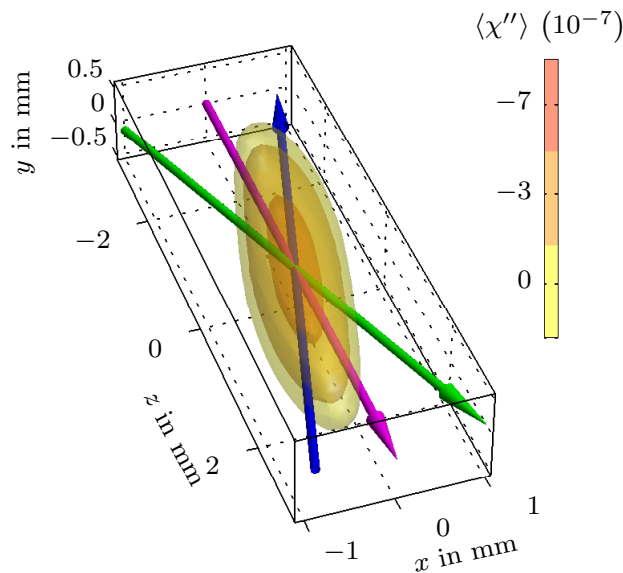


**Figure 5.** Three dimensional gain distribution of the LWI zone for Gaussian beams and realistic laser parameters [2].

### 3. Experimental setup

As the results of the previous section reveal, the most critical parts of the experimental setup of LWI in mercury are the driving lasers at 435.8 nm and 546.1 nm. As mentioned in section 2 special care has been taken to achieve small linewidths. Therefore, the two lasers are devised as frequency doubled external cavity diode lasers (ECDL) with a rugged design.

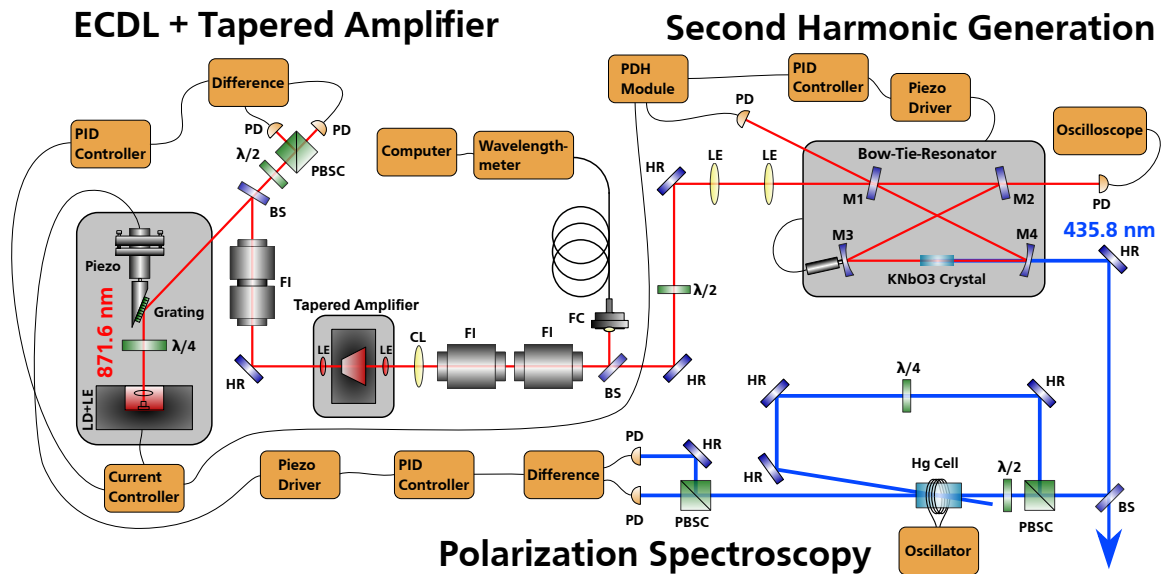


**Figure 6.** Setup of the 435.8 nm laser system. LD: Laser Diode, LE: Lens, BS: Beam sampler, PBSC: Polarizing Beamsplitter Cube, PD: Photo Diode, FI: Faraday Isolator, HR: High Reflecting Mirror, CL: Cylindrical Lens, FC: Fiber Coupler, M1: Input Coupler, M2-M3: High Reflecting Mirrors, M4: Output Coupler for second harmonic radiation. The  $\lambda/4$  and  $\lambda/2$  retarder plates, PBSC and photo diodes in the ECDL sector are used for the locking scheme introduced and discussed in [14].

A schematic view of the laser system producing the 435.8 nm radiation is shown in Fig. 6. The ECDL with a fundamental wavelength of 871.6 nm emits about 30 mW which are boosted up to 1.5 W by a tapered amplifier, while the laser diode is protected from backward radiation by a tandem faraday isolator. A novel locking scheme based on polarization spectroscopy [14] enables a stabilization of the ECDL and mode-hop free tuning up to 22 GHz.

After exiting the tapered amplifier the beam is shaped by a cylindrical lens and then coupled into a four-mirror home-built bow-tie ring resonator, consisting of two plane and two curved mirrors. A 10 mm long potassium niobate ( $\text{KNbO}_3$ ) crystal is placed in the focal spot between the two curved mirrors. This crystal has a very high nonlinear coefficient of  $13.8 \text{ pm V}^{-1}$  and leads to an efficient second harmonic generation. To meet the non-critical phase matching condition the temperature of the  $\text{KNbO}_3$  crystal must be kept very stable. Therefore, the whole resonator is embedded in a solid temperature stabilized aluminum block. Inside the block the  $\text{KNbO}_3$  crystal has its separate temperature stabilization providing a stability of 9 mK over 2 hours at around  $50^\circ\text{C}$ . The resonator itself is stabilized employing the Pound-Drever-Hall technique to the fundamental laser wavelength. The necessary frequency modulation of 20 MHz is directly modulated on the laser diode current through a home-built ultra low-noise current controller. This leads to 204 mW at 435.6 nm with a peak-to-peak stability of 2.2 % over 60 minutes.

The laser system is frequency stabilized on the  $6^3P_1 - 7^3S_1$  transition by polarization spectroscopy in a mercury vapor cell [15]. Since the aforementioned excited states are not populated, a constant gas discharge is induced in the cell to excite the mercury atoms. For this purpose the cell contains argon as a buffer gas at a very small pressure, which helps to ignite the discharge [16]. The circularly polarized pump beam induces an anisotropic saturation of the Zeemann sublevels of the transition. Therefore, the linearly polarized probe beam experiences a slight rotation of the polarization axis while scanning the laser frequency over the atomic

transition. A polarizing beam splitter cube and two photodiodes detect this rotation and the difference of the two signals produces a dispersion like error signal, which is fed back to the ECDL grating piezo actuator through a PID controller. The frequency is stable to within 2.2 MHz peak-to-peak and a standard deviation of 275 kHz over 60 minutes for a 80 ms sampling interval.

The linewidth of the 435.6 nm radiation is measured with a delayed self-heterodyne beating technique [17] with a short delay fiber of about 410 m corresponding to a delay of 2.04  $\mu$ s. Fig. 7 shows a beat-note averaged over 10 measurements; the corresponding fit leads to a short-time linewidth of 24.1 kHz.

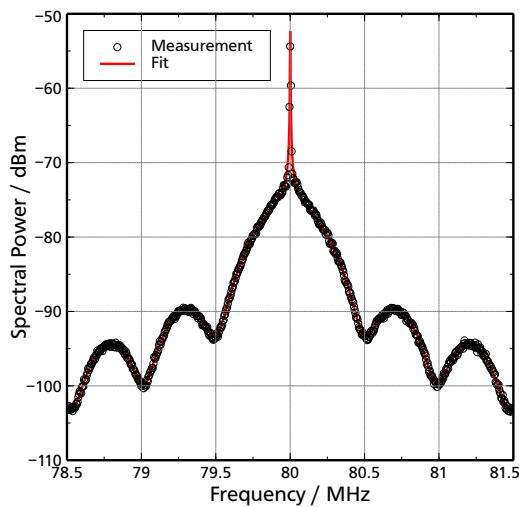


**Figure 7.** Beat-note of the 435.6 nm radiation averaged over 10 measurements, with fitted theory curve as described in [17].

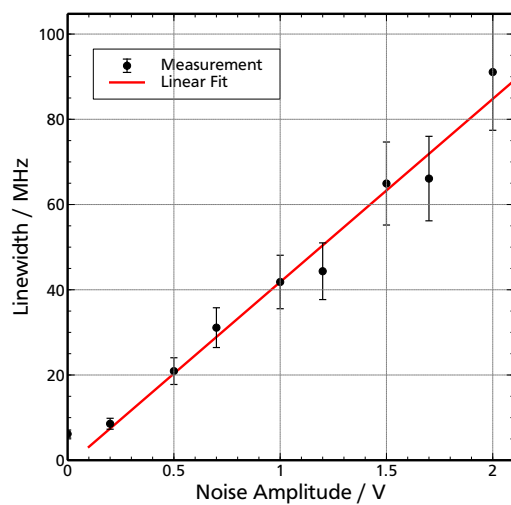


**Figure 8.** Dependence of the linewidth of the 404.7 nm laser on the white-noise modulation amplitude.

The setup of the 546.1 nm laser system is very similar. Because only 2 mW are required at this wavelength, a high-power laser diode in ECDL configuration, which emits 222 mW at the fundamental wavelength, is sufficient. The nonlinear medium for the second harmonic generation is a 20 mm long lithium niobate crystal with 5.5 % magnesium oxide doping ( $\text{MgO}:\text{LiNbO}_3$ ) and a theoretical nonlinear coefficient of  $4.45 \text{ pm V}^{-1}$ . With this configuration we achieved up to 6.3 mW and a conversion efficiency of 7.8 %. The short-time linewidth was measured to be 23.8 kHz.

The incoherent repump laser at 404.7 nm is also based on an ECDL configuration to provide enough power at the desired wavelength for saturating the atomic transition. To broaden the linewidth, the laser diode current is modulated with white-noise directly by a fast-modulation input of our ultra low-noise current controller. In Fig. 8 the dependence of the laser linewidth on the amplitude of the white-noise is shown. The laser frequency is also stabilized in a separate gas discharge by the polarization spectroscopy technique discussed earlier. The system provides up to 25 mW output power.

In order to verify the theoretical model of [1, 2], a laser at 253.7 nm based on fourth harmonic generation will be used to investigate the gain on the LWI lasing transition.

#### 4. Conclusion and outlook

A short summary of our detailed theoretical calculations for lasing without inversion in neutral mercury were presented and the current progress of the experimental realization has been discussed.

The calculations clearly show the feasibility of LWI in mercury and yield the experimental parameters necessary for a successful implementation. The most crucial parameters are the linewidths of the driving lasers.

The presented laser systems meet these demands for the LWI scheme and are ready for first measurements to confirm the calculations of [1, 2]. Currently, we are setting up the gas cell for first measurements of amplification without inversion in neutral mercury.

The authors gratefully acknowledge support by the Deutsche Forschungsgemeinschaft under the research grant "Amplification and Lasing without Inversion in Mercury at 253.7 nm and 185 nm".

#### References

- [1] Fry E S, Lukin M D, Walther T and Welch G R 2000 *Opt. Commun.* **179** 499–504
- [2] Sturm M R, Rein B, Walther T and Wälsler R 2014 *J. Opt. Soc. Am. B* **31** 1964
- [3] Kolbe, Daniel and Scheid, Martin and Walz J 2012 *Phys. Rev. Lett.* **109** 063901
- [4] Watanabe Y Z, Sato Y, Watanabe N, Ananda R, Okada-Shudo Y, Watanabe M, Hyodo M, Wang X, Chen C, Kanai T and Shuntaro 2009 *Opt. Express* **17** 8119–8124
- [5] Mompart J and Corbalán R 2000 *J. Opt. A Pure Appl. Opt.* **2** R7
- [6] Südmeyer T, Imai Y, Masuda H, Eguchi N, Saito M and Kubota S 2008 *Opt. Express* **16** 1546–1551
- [7] Scheid M, Kolbe D and Markert F 2009 *Opt. Express* **17** 11274–11280
- [8] Kocharovskaia O and Khanin Y I 1988 *Pis'ma v Zhurnal Eksp. i Teor. Fiz.* **48** 581–584
- [9] Harris S 1989 *Phys. Rev. Lett.* **62** 1033–1036
- [10] Scully M, Zhu S and Gavrielides A 1989 *Phys. Rev. Lett.* **62** 2813–2816
- [11] Zibrov A S, Lukin M D, Nikonov D E, Hollberg L, Scully M O, Velichansky V L and Robinson H G 1995 *Phys. Rev. Lett.* **75** 1499–1502
- [12] Fry E S 1993 *Phys. Rev. Lett.* **70** 3235
- [13] Padmabandu G, Welch G, Shubin I, Fry E, Nikonov D, Lukin M and Scully M 1996 *Phys. Rev. Lett.* **76** 2053–2056
- [14] Führer T, Stang D and Walther T 2009 *Opt. Express* **17** 4991–4996
- [15] Hughes C P P, Adams C S, Cox S G, Griffin P F, Smith D A and G I 2002 *J. Phys. B At. Mol. Opt. Phys.* **35** 5141–5151
- [16] Veza D, Salit M L, Sansonetti C J and Travis J C 2005 *J. Phys. B At. Mol. Opt. Phys.* **38** 3739–3753
- [17] Führer T and Walther T 2012 *Appl. Phys. B* **108** 249–253